

# Many-body potential and structure for rhodium clusters

Chang-Hong Chien and Estela Blaisten-Barojas<sup>a)</sup>

*Institute for Computational Sciences and Informatics, George Mason University, Fairfax, Virginia 22030*

Mark R. Pederson

*Center for Computational Materials Science, Naval Research Laboratory, Washington DC 20375-5320*

(Received 12 May 1999; accepted 9 November 1999)

The many-body potential for ferromagnetic and paramagnetic rhodium clusters proposed in this work has 11 parameters (14 for the paramagnetic case) that are fitted on the energy surface of  $\text{Rh}_2$  through  $\text{Rh}_6$  clusters calculated from first principles within the generalized gradient approximation (GGA) of density functional theory. Under this potential the most stable ferromagnetic and paramagnetic cluster structures are generated up to  $\text{Rh}_{58}$ . Additionally, the growth under several symmetries is pursued up to  $N=400$ . The face-centered-cubic (fcc) growth path is the most stable at that cluster size regime. An effective measure of the cluster stiffness is calculated as a function of cluster size displaying a monotone increase towards the bulk value. The melting temperature is about constant up to clusters with 45 atoms, presenting a sharp increase towards the bulk value at larger sizes. © 2000 American Institute of Physics. [S0021-9606(00)30805-4]

## I. INTRODUCTION

Structural properties are of fundamental importance for understanding the physical and chemical behavior of clusters. However, there exists no direct experimental method for the determination of the structure of free clusters generated in molecular beams. For that reason, the geometry of clusters is usually inferred indirectly from comparison of measurements that depend on the structure with predictive models and simulations. This approach has been attempted with techniques such as mass spectral abundance,<sup>1</sup> chemical reactivity,<sup>2</sup> magnetism,<sup>3</sup> and electron diffraction.<sup>4</sup>

For transition metal clusters, structural information is becoming available from a wealth of sophisticated experiments. For example, the chemical reactivity of size-selected clusters can be probed by flow-reactor techniques. This method has been used in nickel clusters using nitrogen as the chemical probe. From the experiments it was learned that around  $N=13$  and 55 the geometry is a Mackay icosahedron,<sup>5</sup> whereas for sizes below 55 there are too many possible geometries and multiple isomers might be present.<sup>6</sup> Therefore, it is increasingly important to design reliable structural models to aid the interpretation of experimental data. For transition metal clusters this is a demanding task. While it is now possible to perform *ab initio* calculations on complicated low-symmetry clusters on the order of 100–200 atoms,<sup>7</sup> the *ab initio* determination of many/all low-lying structural isomers in this size regime is not currently in reach. Full *ab initio* searches for structural isomers are certainly limited to 30–50 atoms at this time. The use of sufficiently accurate model potentials can significantly decrease the *ab initio* computational search time by identifying low-energy structures which may then be further investigated within *ab initio* methods. In addition, the Hessian matrices determined from such model potentials should provide for

excellent preconditioning of *ab initio* geometrical optimization methods which further increases the size regime for which *ab initio* methodologies are tenable. Finally, such model potentials<sup>8,9</sup> provide a promising avenue for obtaining structural information and studies of this type also validate the use of such potentials as *ab initio* preconditioners.

Among the 4d transition metals, rhodium clusters display unique magnetic properties exhibiting a richness of spin orderings in small cluster sizes up to about  $N=60$ <sup>3,10,11</sup> despite the fact that bulk rhodium is paramagnetic. Recently, we have performed extensive *ab initio* calculations within the density functional formalism and the generalized gradient approximation (GGA)<sup>12</sup> for small rhodium clusters up to  $\text{Rh}_6$ , where it is shown that magnetic characteristics are associated with the structure as well. Less accurate calculations within the tight binding approximation have reached a similar conclusion.<sup>13</sup>

In this paper we develop a model potential for rhodium clusters and fit its parameters to our previous *ab initio* calculations of  $\text{Rh}_2$  to  $\text{Rh}_6$  ferromagnetic and paramagnetic clusters<sup>12</sup> and use the new potential to determine the structure of rhodium clusters up to  $\text{Rh}_{58}$ . Our results should aid structural assignments from experimental data.

## II. RHODIUM: THE MANY-BODY POTENTIAL AND SMALL CLUSTERS

In 1968, Cyrot-Lackman derived the “moments theorem”<sup>14</sup> which relates the local density of states  $d_i(E)$  for atom  $i$  of a solid to the topology of the local atomic environment and consequently provides a means to represent the binding energy of metals in real space, giving a more chemical flavor to the solid-state physics description in reciprocal space. For example, consider the  $n$ th moment of  $d_i(E)$

<sup>a)</sup>Electronic mail: eblaiste@gmu.edu

TABLE I. Geometry, spin, binding energy, and number of fitting points for the ferromagnetic and paramagnetic electronic states of the rhodium clusters (Ref. 12).

		Ferromagnetic states			Paramagnetic states			
		$S$	$E_b$ (eV)	No. points	$S$	$E_b$ (eV)	No. points	
Rh <sub>2</sub>		2	2.765 (ground)	12	0	1.652 (excited)	11	
Rh <sub>3</sub>	$C_{2v}$	5/2	5.857 (ground)	10	$C_{2v}$	1/2	5.448 (excited)	5
Rh <sub>4</sub>	$D_{4h}$	2	9.481 (excited)	7	$T_d$	0	9.679 (ground)	7
Rh <sub>5</sub>	$C_{4v}$	5/2	13.494 (ground)	21	$C_{4v}$	1/2	13.171 (excited)	13
Rh <sub>6</sub>	$O_h$	3	17.294 (ground)	5	$O_h$	0	17.039 (excited)	5

$$\mu_i^{(n)} = \int_{\text{electronic band}} (E - \epsilon_i)^n d_i(E) dE, \quad (1)$$

where  $\epsilon_i$  is the on-site energy corresponding to the  $i$ th atom. Clearly,  $\mu_i^{(0)} = 1$  if  $d_i(E)$  is normalized,  $\mu_i^{(1)} = 0$  is the center of gravity of  $d_i(E)$  relative to  $\epsilon_i$ , the  $\sqrt{\mu_i^{(2)}}$  represents the width of the local density of states,  $\mu_i^{(3)}$  measures the skewness of  $d_i(E)$ ,  $\mu_i^{(4)}$  indicates when the density becomes bimodal, opening a gap, and higher moments give finer details about the distribution. Additionally, it is not difficult to prove<sup>15</sup> that the moments can be calculated in real space in terms of  $H_{ij}$ , matrix elements of the all electron Hamiltonian spanned on an orthonormal atomic basis set  $|i\rangle$ . In particular,

$$\mu_i^{(2)} = \sum_{j \neq i}^z H_{ij} H_{ji}, \quad (2)$$

is a sum over  $z$  paths, each path representing one electron starting at site  $i$ , hopping out to one of the  $z$  coordination sites  $j$ , and hopping back to  $i$ . Equation (2) emphasizes the importance of the geometry of the local environment to the shape of the local density of states. When the summation is extended to many coordination shells beyond the first neighbors, wiggles are introduced in the functional form of the moments at appropriate places that aid in characterizing the structure of the metal.

Transition metals are elements with a partially filled narrow  $d$  band superimposed on a broad free electron-like  $s-p$  band. The narrowness of the  $d$  band, especially in the  $3d$  series, is a consequence of the relative constriction of the  $d$  orbitals compared with the outer  $s$  and  $p$  orbitals. As one moves across the periodic table, the  $d$  band is gradually being filled. Most of the properties of the transition metals are characterized by the filling of the  $d$  band and ignoring the  $sp$  electrons. This constitutes Fridel's  $d$ -band model<sup>16</sup> which further assumes a rectangular approximation for  $d_i(E)$  such that the bonding energy of the solid is primarily due to the filling of the  $d$  band and proportional to its width. In the second moment approximation (SMA), the bonding energy is then proportional to  $\sqrt{\mu_i^{(2)}}$ . In metals, an important contribution to the structure comes from the repulsive term represented as a sum of pair potentials accounting for the short-range behavior of the interaction between ions.<sup>17</sup> Therefore, the cohesive energy of a transition metal consists of

$$E_{\text{coh}} = E_{\text{rep}} + E_{\text{bond}}. \quad (3)$$

The SMA has been used to suggest various functional forms for interatomic potentials in transition metals such as

the Finnis-Sinclair potential,<sup>18</sup> the closely related embedded atom potential,<sup>19</sup> the tight-binding TB-SMA<sup>20</sup> also referred in the literature as Gupta potential.<sup>21</sup> These potentials differ in the functional representation that is given to the hopping integrals in Eq. (2), because of the summations under the square root they are many-body potentials in the sense that they are not a sum of pairwise additive functions.

The functional form we adopted for rhodium is that of the many-body SMA potential<sup>20-22</sup>

$$E_b = \frac{1}{N} \sum_{i=1}^N \left\{ \epsilon_0 \sum_{j \neq i}^N \exp \left( -p \left[ \frac{r_{ij}}{r_0} - 1 \right] \right) - \left[ \xi_0^2 \sum_{j \neq i}^N \exp \left( -2q \left[ \frac{r_{ij}}{r_0} - 1 \right] \right) \right]^{1/2} \right\}, \quad (4)$$

which has five parameters  $\epsilon_0$ ,  $\xi_0$ ,  $p$ ,  $q$ , and  $r_0$ . The strategy to obtain the values of these parameters is diverse. As for other potentials, the parameters can be fitted to empirical data such as the cohesive energies and elastic constants. Cleri and Rosato<sup>23</sup> fitted these parameters to experimental data for 16 fcc and hexagonal-close-packed (hcp) transition metals. Their parameters for rhodium are: 0.0629 eV, 1.66 eV, 18.45, 1.867,  $a/\sqrt{2}$  ( $a=3.803$  Å), respectively. These bulk fcc parameters give a cohesive energy of 5.752 eV, elastic constants of  $C_{44}=1.99$  Mbar,  $C_{11}-C_{12}=1.55$  Mbar, and a bulk modulus of 2.89 Mbar. A different parametrization strategy was introduced by Sigalas and Papacostantopoulos<sup>22</sup> in which the parameters were fitted to local density approximation (LDA) calculations of the total energy as a function of lattice constant. Their parameters for rhodium are 0.0911 eV, 3.823 eV, 9.22, 2.302, 3.215 Å.

For Rh clusters we propose an alternative parametrization based on a simultaneous fit to the energy surfaces of clusters, Rh<sub>2</sub> through Rh<sub>6</sub>, obtained from our recent GGA calculations.<sup>12</sup> Two sets of electronic states are identified from those calculations as summarized in Table I. In the first set, the spin multiplicity is high, indicating that many of the valence electrons have unpaired spins. This set is referred to as *ferromagnetic* and contains 12, 10, 7, 31, and 5 different geometries of Rh<sub>2</sub>, Rh<sub>3</sub> ( $C_{2v}$ ,  $S=5/2$ ), Rh<sub>4</sub> ( $D_{4h}$ ,  $S=2$ ), Rh<sub>5</sub> ( $C_{4v}$ ,  $S=5/2$ ), and Rh<sub>6</sub> ( $O_h$ ,  $S=3$ ), respectively. In the second set, the electronic states have the lowest possible spin multiplicity corresponding to valence electrons with paired spins. This set is called *paramagnetic*, containing either singlets for clusters with even number of atoms and doublets for clusters with odd number of atoms. The paramagnetic set contains 11 different geometries of the dimer in

TABLE II. Parameters of the SMA potential fitted on GGA calculations for the paramagnetic and ferromagnetic energy states.

	Paramagnetic parameters		Ferromagnetic parameters
	Even $N$	Odd $N$	
$X_{\xi_0}$	2.172 810	2.865 745	1.382 924
$X_{\epsilon_0}$	1.329 564	1.930 130	1.667 817
$X_{r_0}$	1.024 129	0.395 899	1.069 258
$\xi_{0\text{dimer}}$ (eV)	0.943 363		1.520 022
$\epsilon_{0\text{dimer}}$ (eV)	0.118 447		0.134 767
$r_{0\text{dimer}}$ (Å)	2.301 889		2.330 994

the  $S=0$  state, 7 different geometries of  $\text{Rh}_4$  ( $T_d$ ,  $S=0$ ), 5 configurations of  $\text{Rh}_6$  ( $O_h$ ,  $S=0$ ), 5 geometries of  $\text{Rh}_3$  ( $C_{2v}$ ,  $S=1/2$ ), and 13 geometries of  $\text{Rh}_5$  ( $C_{4v}$ ,  $S=1/2$ ),

Therefore, two sets of parameters can be produced, one associated to the fit to the ferromagnetic electronic states, and another corresponding to the fit to the paramagnetic electronic states. In both sets the two parameters  $p=18.450$  and  $q=1.867$  representing the range of the repulsive and attractive part of the potentials are kept fixed and equal to the bulk fcc rhodium parameters proposed in Ref. 23. This is a reasonable assumption because the range of the interactions should not be correlated to the magnetic characteristics of the material but rather to its metallic character. Regarding the remaining three parameters,  $\epsilon_0$ ,  $\xi_0$ ,  $r_0$ , it was not possible to obtain a reasonable single fit on either of the two sets of electronic states. Instead, we discovered a size dependence ( $N$ ) of these three parameters revealing the following law:

$$F(N) = (F_{\text{dimer}} - F_{\text{fcc}}) \left( \frac{2}{N} \right)^{X_F} + F_{\text{fcc}}, \quad (5)$$

where  $F$  is either  $\xi_0$ ,  $\epsilon_0$ , or  $r_0$ ;  $F_{\text{fcc}}$  are the bulk values of Ref. 23. The  $F_{\text{dimer}}$  correspond to ferromagnetic or paramagnetic parameters fitted to our GGA calculations for the dimer only (12 points in the  $S=2$  state for the ferromagnetic set and 11 energy points in the  $S=0$  state for the paramagnetic set). The exponents  $X_F$  were fitted using the Levenberg–Marquart algorithm on cluster geometries for  $3 \leq N \leq 6$  corresponding to the ferromagnetic or paramagnetic sets. With this parametrization, the SMA potential has 11 parameters for the ferromagnetic clusters. For the fit to paramagnetic states, it was necessary to consider three exponents for the clusters with even  $N$  and three different exponents for clusters with odd  $N$ . Therefore, the total number of parameters for the paramagnetic case is 14. These parameters are reported in Table II. For the ferromagnetic potential, the relative error of the fit is 3% on the energy of 55 points distributed over the five different ferromagnetic energy surfaces of Table I. For the even-paramagnetic potential, the relative error of the fit is 3% on the energy of 55 points distributed over the five different ferromagnetic energy surfaces of Table II. For the even-paramagnetic potential the relative error over 23 points is 5% and for the odd-paramagnetic potential it is 1%.

To verify the validity of the proposed SMA potential we calculated the total binding energy for high-symmetry  $O_h$  clusters ( $N=12, 13, 24, 25$ , and 48) within the SMA poten-

TABLE III. Binding energy per atom  $E_b$  (eV) and bond length  $r_e$  (Å) of Rh clusters within the many-body SMA potential (unrelaxed and relaxed), and the first-principles GGA and LDA.

Sym.	Spin	SMA (unrelaxed) $E_b$	GGA		LDA		SMA (relaxed)	
			$r_e$	$E_b$	$r_e$	$E_b$	$r_e$	$E_b$
$\text{Rh}_{12}$	$O_h$	0	3.299	2.574 2.918	2.484 3.794	2.569 3.325		
$\text{Rh}_{13}$	$O_h$	1/2	3.739	2.664 3.030	2.591 3.867	2.631 3.749		
$\text{Rh}_{24}$	$O_h$	0	3.313	2.446 3.251	2.367 4.290	2.574 3.452		
$\text{Rh}_{25}$	$O_h$	1/2	3.398	2.464 3.327	2.390 4.280	2.572 3.478		
$\text{Rh}_{48}$	$O_h$	0	2.877	2.441 2.920	2.428 3.681	2.574 2.965		

tial, the *ab initio* GGA, and local density approximation (LDA) methods.<sup>12</sup> The optimized bond lengths and binding energies are listed in Table III. These  $O_h$  clusters are not the isomers with lowest energy, but rather are high-energy isomers that were chosen because of the feasibility of the GGA and LDA calculations at the same level of sophistication as described in Ref. 12. As seen from the table, the agreement is excellent. The differences in the binding energy between the GGA and the SMA potential range from 1.5% to 23% (columns 4 and 6). If the SMA potential configurations are allowed to relax, then the energy differences increase slightly (columns 6 and 10) but discrepancies of 0.2% to 5.4% in the shortest bond distance develop (see columns 5 and 9). The relaxation of these structures gave very shallow minima that do not necessarily maintain the  $O_h$  symmetry. In general, the differences between our SMA and GGA cohesive energies are smaller than the differences between the LDA and GGA cohesive energies (see columns 7 and 8). This is good proof for the model potential, showing that is more appropriate than LDA calculations.

### III. STRUCTURE OF RHODIUM CLUSTERS

Subsequently, the most stable geometries of clusters with sizes up to 58 were discovered via an unrestricted Monte Carlo method<sup>8</sup> supplemented with a genetic algorithm optimization.<sup>24</sup> For each size, 1000 random trials within a volume consistent with close packing, led to a distribution of minima out of which an optimization using genetic algorithms gave the global minimum. Typical distributions of different minima (with binding energies/atom differing in the third decimal) for clusters with  $N=19, 26, 31, 38, 48$ , and 55 are illustrated in Fig. 1. The histograms were built with approximately 1000 minima for each size (700 in the case of  $\text{Rh}_{19}$ ). Most of the low-energy minima have icosahedral, decahedral, or hexagonal closed-packed (hcp) motifs. It is clearly seen that the  $O_h$  structures of Table III are very low binding energies isomers.

Tables IV and V contain the energies of the configurations corresponding to the global minimum of ferromagnetic and paramagnetic clusters, respectively. The structure of almost all clusters is either that reported for Lennard-Jones potentials<sup>25</sup> or for the Sutton–Chen 12–6 potential<sup>26</sup> except for ferromagnetic and paramagnetic  $\text{Rh}_{24}$  and  $\text{Rh}_{45}$  shown in Fig. 1 (top). This is indicated in the table by LJ and SC.  $\text{Rh}_{24}$  is the  $\text{Rh}_{19}$  (capped icosahedron) with five adjacent faces

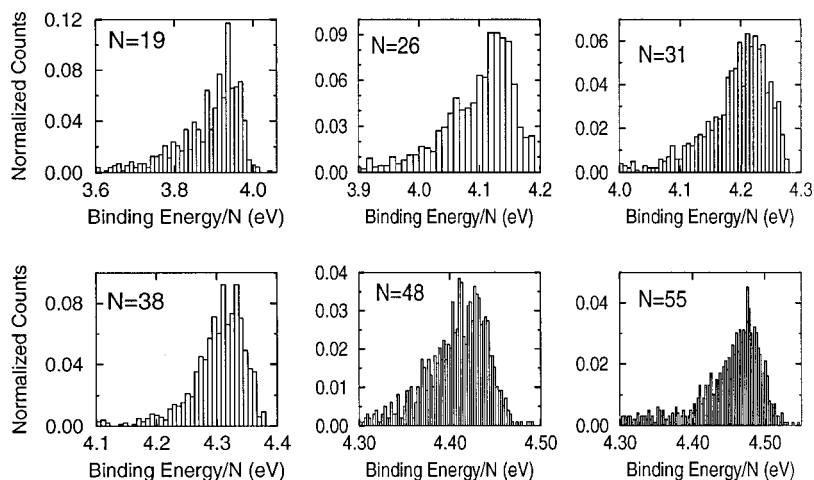


FIG. 1. Normalized histograms of the binding energy per atom of different isomers of rhodium clusters with  $N=19, 26, 31, 38, 48,$  and  $55$  collected from the Monte Carlo simulation.

decorated with one atom. Different combinations to decorate five faces of the  $\text{Rh}_{19}$  structure give rise to a group of isomers with very close binding energies. Among other  $\text{Rh}_{24}$  isomers close to the global minimum is an interesting structure (shown in Fig. 2 center) composed of two icosahedra sharing one face plus one atom decorating a face adjacent to the shared face. The most stable structures for  $\text{Rh}_{13}$  and  $\text{Rh}_{55}$  are Mackay icosahedra;<sup>5</sup>  $\text{Rh}_{38}$  is the truncated octahedron. At other cluster sizes, hcp and fcc motifs can be identified. For example, ferromagnetic  $\text{Rh}_{26}$  and  $\text{Rh}_{48}$  are hcp clusters as shown in Fig. 2 (bottom).

The average bond distance increases slowly, changing from 2.55 to 2.68 Å for ferromagnetic  $\text{Rh}_7$  through  $\text{Rh}_{58}$ . In contrast, the paramagnetic clusters present a slight contrac-

tion of the average bond length, changing from 2.6 to 2.54 Å in the same size range (the bond length in bulk rhodium is 2.689 Å). A given experimental sample of rhodium clusters might be a mixture of ferromagnetic and paramagnetic clusters. It would be interesting to separate them experimentally. Additionally, since there are dozens of minima within a hundredth of an eV, these isomers can be attained within thermal energies. It is expected that experiments based on the stability of clusters (such as mass spectra) will be strongly masked by the broad distribution of isomers. This pattern has been observed experimentally by mass spectrometry,<sup>27</sup> where no outstanding features could be recognized from the spectra of rhodium clusters in the size range studied here. It is worth noting that these experiments did not separate ferromagnetic

TABLE IV. Binding energy  $E_b$  per atom of ferromagnetic Rh clusters with the many-body SMA potential.

Size	$E_b$	Potential	Size	$E_b$	Potential
7	3.209	SC,LJ	33	4.324	SC
8	3.308	SC,LJ	34	4.332	LJ
9	3.424	SC,LJ	35	4.354	SC
10	3.523	SC,LJ	36	4.371	SC,LJ
11	3.604	SC,LJ	37	4.384	SC
12	3.709	SC,LJ	38	4.414	SC,LJ
13	3.844	SC,LJ	39	4.424	LJ
14	3.843	SC,LJ	40	4.429	SC,LJ
15	3.884	SC,LJ	41	4.434	LJ
16	3.917	SC,LJ	42	4.446	SC,LJ
17	3.946	SC,LJ	43	4.461	SC,LJ
18	3.986	LJ	44	4.466	SC,LJ
19	4.054	SC,LJ	45	4.479	this work
20	4.068	SC,LJ	46	4.499	SC,LJ
21	4.082	SC	47	4.502	SC,LJ
22	4.106	LJ	48	4.514	LJ
23	4.150	LJ	49	4.532	SC,LJ
24	4.157	this work	50	4.535	LJ
25	4.172	SC,LJ	51	4.594	SC
26	4.203	LJ	52	4.566	SC
27	4.214	LJ	53	4.581	SC
28	4.239	SC	54	4.596	SC,LJ
29	4.250	SC	55	4.610	SC,LJ
30	4.269	SC	56	4.602	SC,LJ
31	4.288	SC	57	4.599	SC,LJ
32	4.314	SC,LJ	58	4.607	SC,LJ

TABLE V. Binding energy  $E_b$  per atom of paramagnetic Rh clusters with the many-body SMA potential.

Size	$E_b$	Potential	Size	$E_b$	Potential
7	3.241	SC,LJ	33	4.335	SC
8	3.266	SC,LJ	34	4.331	LJ
9	3.459	SC,LJ	35	4.365	SC
10	3.498	SC,LJ	36	4.3670	SC,LJ
11	3.637	SC,LJ	37	4.394	SC
12	3.692	SC,LJ	38	4.413	SC,LJ
13	3.874	SC,LJ	39	4.433	LJ
14	3.831	SC,LJ	40	4.428	SC,LJ
15	3.911	SC,LJ	41	4.443	LJ
16	3.908	SC,LJ	42	4.445	SC,LJ
17	3.970	SC,LJ	43	4.469	SC,LJ
18	3.979	LJ	44	4.464	SC,LJ
19	4.076	SC,LJ	45	4.487	this work
20	4.063	SC,LJ	46	4.498	SC,LJ
21	4.101	SC	47	4.510	SC,LJ
22	4.101	LJ	48	4.513	LJ
23	4.167	LJ	49	4.539	SC,LJ
24	4.153	this work	50	4.534	LJ
25	4.189	SC,LJ	51	4.556	SC
26	4.200	LJ	52	4.565	SC
27	4.228	LJ	53	4.588	SC
28	4.237	SC	54	4.595	SC,LJ
29	4.263	SC	55	4.617	SC,LJ
30	4.267	SC	56	4.601	SC,LJ
31	4.300	SC	57	4.604	SC,LJ
32	4.312	SC,LJ	58	4.606	SC,LJ

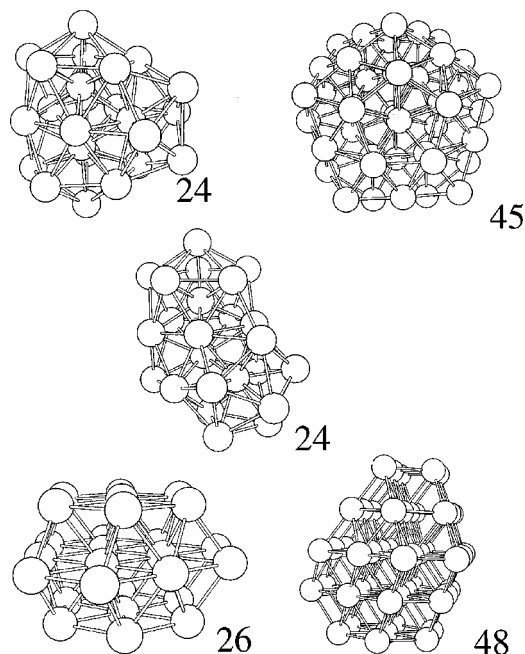


FIG. 2. Most stable geometries of ferromagnetic and paramagnetic  $Rh_{24}$ ,  $Rh_{45}$  (top), a low-energy  $Rh_{24}$  isomer (center), and most stable geometries of ferromagnetic  $Rh_{26}$ ,  $Rh_{48}$  (bottom); both are hcp structures.

from paramagnetic clusters and the estimated temperatures were high enough to allow for the presence of many isomers other than those corresponding to the global minimum.

$Rh_{13}$ LDA calculations yield the icosahedron as the most stable isomer.<sup>28</sup> Comparison of the results in Table IV and V with the tight binding calculations of Ref. 13 reveal that the geometries for  $N=13, 15, 17, 19, 20, 23, 27, 43,$  and  $51$  reported in that paper as the most stable are not minimum energy configurations.

#### IV. DISCUSSION

A qualitative description of the packing behavior of larger clusters is investigated by following the cluster growth under a fixed symmetry. To that purpose, spherical clusters with 20 and up to 400 atoms were cut from either fcc or hcp lattices and relaxed under the SMA potential with the conju-

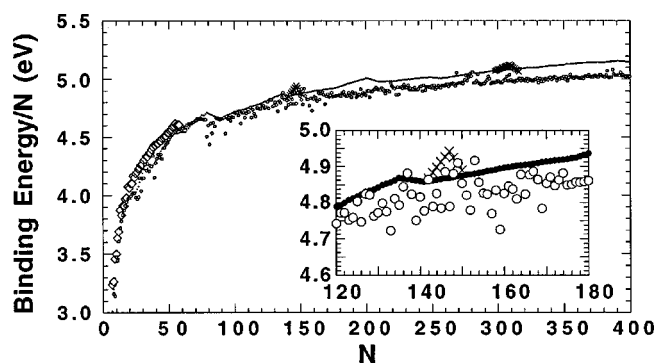


FIG. 3. Binding energy per atom of cluster isomers restricted to a given symmetry compared to the results of Tables IV and V (diamonds) as a function of cluster size: circles: fcc clusters; dots: hcp clusters; crosses: Mackay icosahedra, complete and incomplete.

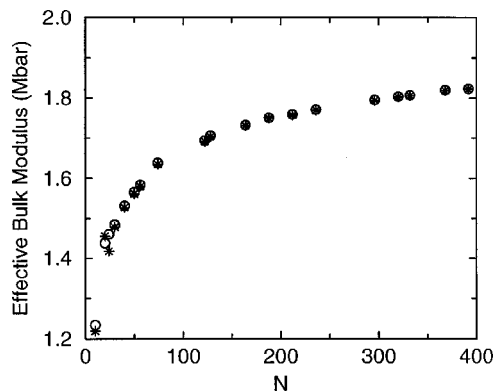


FIG. 4. Effective bulk modulus as a function of cluster size: circles: ferromagnetic clusters; asterisks: paramagnetic clusters.

gate gradient method. Results are shown in Fig. 3, where the diamonds stand for the ferromagnetic SMA results reported in Tables IV and V, the black circles indicate the relaxed fcc clusters, and the small dots stand for relaxed hcp clusters. In addition, the crosses indicate just a few cluster sizes around the Mackay icosahedra properly relaxed under the SMA. It is clear that the cluster growth beyond  $N=56$  will continue to have mixed symmetry components, with perhaps a less important hcp ingredient as the size increases. It is also evident that the fcc packing becomes notoriously more stable for clusters with more than 300 atoms.

In order to describe the elastic behavior of these clusters, we define an effective bulk modulus as

$$B_{\text{eff}}(N) = v_{\text{eff}} \partial^2 E_b / \partial v_{\text{eff}}^2, \quad (6)$$

where the effective volume per atom is  $v_{\text{eff}} = 4\pi r_{\text{avg}}^3 / 3$  and  $r_{\text{avg}}$  is the average bond length. Figure 4 shows the trend of the effective bulk modulus as a function of cluster size. This property increases rapidly for cluster sizes below  $N=50$ , showing that the smaller clusters require little energy to produce a given deformation. Figure 4 contains information related to isomers in the global minimum up to  $N=58$ , and from there on the geometries considered were primarily the fcc structures reported in Fig. 3. The differences between ferromagnetic and paramagnetic clusters are very small. However, for very small sizes up to  $Rh_{25}$  the behavior is significantly different. For example, paramagnetic  $Rh_{24}$  is stiffer than the ferromagnetic cluster. At size 19 this behavior reverses. Overall, a sharp increase in the effective bulk modulus occurs at small sizes  $N < 50$ , and a smoother increase towards the bulk value is apparent above this size.

The ease of deformation of the smaller clusters is due to the fact that atoms in the cluster behave much like the atoms in the first layer of the closest packed fcc infinite surface. In fact, using the SMA bulk parameters of Ref. 23, the surface energy of  $Rh(111)$ , defined as the energy/atom calculated for atoms relaxed on the first (outermost) layer, second layer, third layer, etc., is  $-4.96, -5.71, -5.78,$  and  $-5.79$  eV, respectively. Inner layers beyond the fourth layer contribute as bulk ( $-5.752$  eV). The surface layers have an interlayer relaxation of  $-0.03\%, -0.1\%$ , for the first two, and a positive small relaxation of about  $0.002\%$  for the next two inner layers, which is consistent with experiments.<sup>29</sup> As a compari-

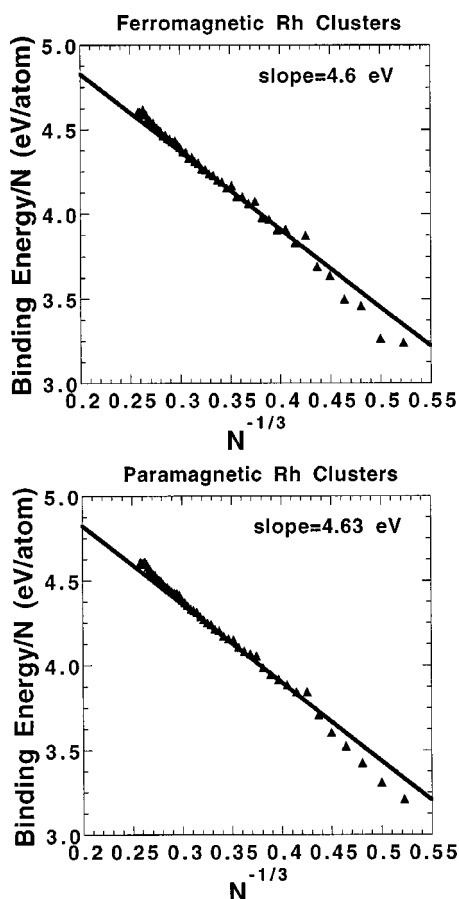


FIG. 5. Binding energy per atom as a function of  $N^{-1/3}$  for ferromagnetic and paramagnetic clusters.

son, for clusters an equivalent quantity can be calculated from the slope of the binding energy as a function of  $N^{-1/3}$ . Figure 5 shows these plots for the ferromagnetic and paramagnetic clusters. The corresponding slopes are 4.6 and 4.63 eV for ferromagnetic and paramagnetic clusters, respectively. This indicates that the full binding energy in the cluster has the character of surface energy.

Some of the equilibrium thermodynamic properties of the isomers reported in Tables IV and V can be analyzed with molecular dynamics (MD). For example, Fig. 6 illustrates the trend of the melting temperature as a function of

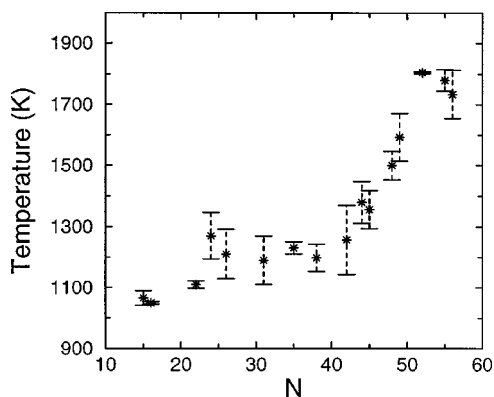


FIG. 6. Melting temperature as a function of cluster size for the ferromagnetic clusters.

cluster size. In these simulations the internal energy was calculated as a function of temperature. From plots of internal energy vs temperature, the melting temperature was identified as the midpoint of the region where a change of slope takes place.<sup>30</sup> The error bars indicate the width of the transition region. As is apparent from the figure, the melting temperature is roughly 1200 K up to sizes of about 45, and then increases, remaining below the bulk value of 2258 K.

## V. CONCLUSION

In this paper we have applied a large-scale computer simulation to reveal that a many-body potential does indeed model well the structure of rhodium clusters. A crucial feature is that the parameters of this potential depend on the size of the cluster. The minimum energy structure of ferromagnetic and paramagnetic clusters is not always the same. In addition, there is strong evidence that the fcc packing starts dominating the growth at sizes on the order of 300 atoms, contrary to the 10 000 expected for van der Waals clusters.<sup>31</sup> Furthermore, it is demonstrated that the stiffness of Rh clusters is about half the bulk value and increases as a smooth function of size, changing by 50% in the size range 10 to 400. This smooth change is indicative that atoms in the clusters behave much as the atoms in the first two to three layers of an infinite surface. Finally, the melting temperature as a function of cluster size is about half the value of the bulk up to sizes  $N=50$ , and starts increasing for larger sizes.

## ACKNOWLEDGMENT

E.B.B. acknowledges the support from the Institute for Computational Sciences and Informatics at George Mason University allocated to C.H.C.'s research assistantship.

- <sup>1</sup>T. P. Martin, Phys. Rep. **273**, 199 (1996).
- <sup>2</sup>S. J. Riley, in *Clusters of Atoms and Molecules II*, edited by H. Haberland (Springer Berlin, 1994), p. 221.
- <sup>3</sup>A. J. Cox, J. G. Louderback, S. E. Apsel, and L. A. Bloomfield, Phys. Rev. B **49**, 12295 (1994).
- <sup>4</sup>J. Farges, M. F. de Feraudy, B. Raoult, and G. Torchet, Adv. Chem. Phys. **70**, 45 (1988).
- <sup>5</sup>A. L. Mackay, Acta Crystallogr. **15**, 916 (1962).
- <sup>6</sup>E. K. Parks, G. C. Niemann, K. P. Kerns, and S. J. Riley, J. Chem. Phys. **107**, 1861 (1997).
- <sup>7</sup>M. R. Pederson and S. N. Khanna, Phys. Rev. B **60**, 9566 (1999).
- <sup>8</sup>E. Blaisten-Barojas and S. N. Khanna, Phys. Rev. Lett. **61**, 1477 (1988).
- <sup>9</sup>Y. Li, E. Blaisten-Barojas, and D. Papaconstantopoulos, Phys. Rev. B **57**, 15519 (1998).
- <sup>10</sup>R. J. Van Zee, Y. M. Hamrick, S. Li, and W. Weltner, Jr., Chem. Phys. Lett. **195**, 214 (1992).
- <sup>11</sup>A. J. Cox, J. G. Louderback, and L. A. Bloomfield, Phys. Rev. Lett. **71**, 923 (1993).
- <sup>12</sup>C. H. Chien, E. Blaisten-Barojas, and M. R. Pederson, Phys. Rev. A **58**, 2196 (1998).
- <sup>13</sup>P. Villaseñor-González, J. Dorantes-Dávila, H. Dreyssé, and G. M. Pastor, Phys. Rev. B **55**, 15084 (1997).
- <sup>14</sup>F. Cyrot-Lackmann, J. Phys. Chem. Solids **29**, 1235 (1968).
- <sup>15</sup>A. Sutton, *Electronic Structure of Materials* (Clarendon, Oxford, 1993), p. 68.
- <sup>16</sup>J. Fridel, Adv. Phys. **3**, 446 (1954).
- <sup>17</sup>D. G. Pettifor, Solid State Phys. **40**, 43 (1987).
- <sup>18</sup>M. W. Finnis and J. E. Sinclair, Philos. Mag. **50**, 45 (1984).
- <sup>19</sup>M. S. Daw and M. I. Baskes, Phys. Rev. B **29**, 6443 (1984).
- <sup>20</sup>W. Zhong, Y. S. Li, and D. Tomaneck, Phys. Rev. B **44**, 13053 (1991).
- <sup>21</sup>R. P. Gupta, Phys. Rev. B **23**, 6265 (1985).

- <sup>22</sup>M. M. Sigalas and D. A. Papaconstatopoulos, *Phys. Rev. B* **49**, 1574 (1994).
- <sup>23</sup>F. Cleri and V. Rosato, *Phys. Rev. B* **48**, 22 (1993).
- <sup>24</sup>G. Wang, A. Roitberg, and E. Blaisten-Barojas (unpublished).
- <sup>25</sup>D. J. Wales and J. P. K. Doye, *J. Phys. Chem. A* **101**, 5111 (1997).
- <sup>26</sup>D. J. Wales and J. P. K. Doye, *New J. Chem.* **22**, 733 (1998).
- <sup>27</sup>T. P. Martin (private communication).
- <sup>28</sup>J. Yang, F. Toigo, K. Wang, and M. Zhang, *Phys. Rev. B* **50**, 7173 (1994).
- <sup>29</sup>A. Eichler, J. Hafner, G. Kresse, and J. Furthmüller, *Surf. Sci.* **352–354**, 689 (1996).
- <sup>30</sup>I. L. Garzón, M. Avalos-Borja, and E. Blaisten-Barojas, *Phys. Rev. B* **40**, 4749 (1989).
- <sup>31</sup>J. A. Northby, *J. Chem. Phys.* **87**, 6166 (1987).